Centennial-scale intensification of wet and dry extremes in North America

Kyungmin Sung[1], Gil Bohrer[1], James Stagge[1]

[1]Civil, Environmental and Geodetics Engineering, The Ohio State University, Columbus, Ohio

Corresponding author: James Stagge (stagge.11@osu.edu)

Key Points:

- This study models seasonal drought and pluvial trends, merging reconstructions, observations, and projected from 850 to 2100 CE.
- Results show widespread exacerbation of both extremes with overall drying (wetting) in the southern (northeastern) North America.
- Modern drought and pluvial distributions are outside pre-Industrial (1850) conditions, and exhibiting substantial shifts in some regions.

Abstract

Drought and pluvial extremes are defined as deviations from typical climatology; however, the background climatology can shift over time in a non-stationary climate, impacting interpretations of extremes. This study evaluated changes in meteorological drought and pluvial extremes by merging tree-ring reconstructions, observations, and climate-model simulations spanning 850 – 2100 CE across North America to determine whether the Industrial era and projected future lie outside the range of natural climate variability. Our results found widespread and spatially consistent exacerbation of both extremes, especially summer drought and winter pluvials, with west and south drying, the northeast wetting trends, and increased interannual variability across the east and north. Our study underscores climate change has already shifted precipitation climatology beyond pre-Industrial climatology and is projected to further intensify ongoing shifts.

Plain Language Summary

Managing water resources has become challenging due to effect of human-caused climate change on extremes. This study examines trends in droughts and pluvials (extreme wet periods) from the distant past (850 CE) to the projected future (2100 CE) to determine whether precipitation extremes in the modern, Industrial era and the future are beyond what is typical of natural climate variability in North America. Gradual precipitation trends were generated by merging information from tree rings, observations, and climate models using a novel statistical approach to correct bias. Results indicate the widespread intensification of both drought and pluvials – especially summer drought and winter pluvials during the modern and future periods. Spatially, southern and western regions are becoming drier, while the northeast is getting wetter, and intermediate regions show a wider range between drought and pluvial years. Our study suggests that anthropogenic climate change has already modified drought and pluvial extremes beyond natural, pre-Industrial conditions and these ongoing trends are projected to intensify through the future. Wider ranges between extreme dry and wet years increases risk for water management and shows the need for adapting water strategies to account for the "new normal" of the climate change.

1. Introduction

Quantifying precipitation non-stationarity is particularly important given the impact of anthropogenic climate change overlaid onto longer patterns of natural climate variability (Stahle et al., 2020; Williams et al., 2022). Future hydroclimate projections indicate intensifying extremes, such as droughts or pluvials (periods with sustained high precipitation) for many regions, shifting what was historically extreme to become more commonplace (Ault, 2020; Bishop et al., 2021; Stevenson et al., 2022). This has critical implications for water management systems and policies designed using early 20th century climate baselines, which may no longer be representative of current or future hydroclimate, increasing risk and vulnerability.

Some regions have already experienced such changes. Mean annual precipitation in the eastern US has generally increased over the past century, while that of western US has decreased, with those changes during the past 100 years likely the most rapid since 1400CE (B. Cook et al., 2019; Williams et al., 2022). These trends are attributed to anthropogenic global warming combined with complex natural variability (Diffenbaugh et al., 2015, 2017; Hoylman et al., 2022; Lehner et al., 2017), which can be better understood when placed in the context of centuries of pre-Industrial natural variability.

This study merges tree-ring proxy reconstructions, gridded observations, and Global Climate Model (GCM) output to quantify climate non-stationarity at a centennial-scale, permitting an estimation of anthropogenic climate change impacts on drought and pluvials relative to natural pre-Industrial variability. Modern observations often extend a century into the past, while tree-ring reconstructions can extend more than 1000 years (Bishop et al., 2021), and GCMs can simulate climate over centuries from the distant past through feasible future emissions scenarios (Marvel et al., 2021). Merging these datasets creates challenges due to unique biases, stemming from tree growth sensitivities in reconstructions and systematic model biases in GCMs (Cui et al., 2021). Additionally, temporal and spatial resolution differences complicate the creation of a merged series. For example, the North American Seasonal Precipitation Atlas (NASPA) proxy reconstruction used here provides bi-annual precipitation estimates, comprised of one 5-month cool season and one 3-month warm season (Stahle et al., 2020); far coarser than daily or monthly resolution of the other datasets.

Hence, this study aims to address: (1) whether future projections of wet and dry precipitation extremes are significantly different from the past 1000 years, and (2) how trends during the instrumental period (1900 – 2020CE) fit into the longer pattern of natural climate variability and anthropogenic climate change. This is accomplished through a novel non-linear spline model (Stagge & Sung, 2022; Sung et al., 2022) which simultaneously corrects data-induced bias to generate a single, common model of century-scale shifts in the 3-month Standardized Precipitation Index (SPI-3) (Heim, 2002), representing drought and pluvial extremes.

2. Methods

2.1. Data

Precipitation estimates were based on tree-ring reconstructions (NASPA), processed gridded observations (CRU and GridMET), and two CMIP6 model simulations (MRI-ESM2-0 and MIROC-ES2L, Table 1) . Two CMIP6 models were chosen because they provide simulations of the full period 850-2100 CE via the *past1000* (850 to 1849 CE), *historical* (1850 to 2014 CE), and *ScenarioMIP* experiments (2015-2100 CE). We considered two future Socioeconomic Shared Pathways (SSPs) to bracket potential futures from the "business as usual" high emissions scenario, SSP 5-8.5, to the low emissions scenario, SSP1-2.6 (Eyring et al., 2016).

Table 1. Datasets.

Name	Model	CMIP6 Experiment	Period	Spatial Resolution
CRU	Observed	-	1901-2018	0.5° × 0.5° (Harris et al., 2020)
GridMET+	Observed	-	1950 - 2020	0.04° × 0.04° (Abatzoglou, 2013)
NASPA	Proxy + Downscaled	-	850* - 2016	0.5° × 0.5° (Stahle et al., 2020)
MIROC-ES2L	GCM	Past1000	850-1849	2.8° × 2.8° (Hajima et al., 2020)
MIROC-ES2L	GCM	Historical	1850- 2014	2.8° × 2.8° (Hajima et al., 2020)
MIROC-ES2L	GCM	SSP1-2.6 & SSP5-8.5	2015- 2100	2.8° × 2.8° (Hajima et al., 2020)
MRI-ESM2	GCM	Past1000	850 - 1849	100 km × 100 km (Yukimoto et al., 2019)
MRI-ESM2	GCM	Historical	1850 -2014	100 km × 100 km

				(Yukimoto et al., 2019)
MRI-ESM2	GCM	SSP1-2.6 & SSP5-8.5	2015- 2100	100 km × 100 km (Yukimoto et al., 2019)

*NASPA starting year varies from 0-1400 C.E., depending on the grid location. This study used data from 850 C.E. if it were available.
[+]US only

Spatial resolution followed NASPA grid placement and resolution (0.5° x 0.5°) with relevant time series from the other datasets selected based on the shortest distance to the NASPA grid center. GridMET data is only available for the Continental United States, so was not included outside this region.

2.2. Temporal Downscaling

Precipitation was considered at a monthly resolution, natively for all datasets except for the bi-annual NASPA, which was temporally downscaled following the approach of Sung and Stagge (2022) using K-nearest neighbor (KNN) resampling (Gangopadhyay et al., 2005). Here, KNN resampling was used to insert 13-month SPI-3 series from the observed record into a given NASPA year based on similarity to the 3 bracketing NASPA estimates (prior year's MJJ, concurrent DJFMA, and concurrent MJJ). Global Precipitation Climatology Centre (GPCC) precipitation was used as the historical catalog because it was originally used for NASPA calibration.

KNN resampling used SPI-3 sequences, then converted to precipitation, rather than precipitation sequences. This increased the sampling catalog twelve-fold, avoiding repetition in resampling, and was reasonable because normalized SPI-3 values are independent of season. Ten annual historical SPI-3 sequences were resampled (K=10), converted back to precipitation, and then averaged to produce the monthly NASPA estimate and associated uncertainty.

2.3. Non-Stationary SPI

A non-stationary SPI (NSPI) approach (Sung et al., 2022) was used to simultaneously model centennial-scale trends of droughts and pluvials and to account for data-induced bias. The NSPI is similar to the the SPI by fitting probability density functions to accumulated precipitation, but allows distribution parameters to shift gradually through time (Pedersen et al., 2019; Wood, 2008). The two parameters of the gamma distribution (mean, μ and shape, α) were modeled simultaneously by month and year to simultaneously capture recurring seasonality (monthly) and

multi-decadal trends (year) (Eqs. 1-3). Here, $P_{3-month,m,y}$ represents the 3-month average precipitation rate at month *m* and year *y*. This model therefore captures shifts in the underlying distribution, from which we can extract changes in drought and pluvials, defined as SPI= -1.5 (percentile = 6.7%) and SPI = 1.5 (percentile = 93.3%), respectively.

To account for data bias in the mean (Eq 2) and shape (Eq 3) parameters, the model included a unique intercept, β_0, and a spline function to account for seasonally differing biases, $\beta_1 f_s$. The function *fs* is a cubic polynomial spline controlled by β at each control point. The final term, $f_{te}(X_{year}, X_{month})$, represents the common smoothed long-term trend and seasonality after accounting for biases, modeled as a tensor product spline function.

$$P_{3\,month,m,y} = gamma(\mu, \alpha) \quad \begin{pmatrix} m: month, \\ y: year \end{pmatrix} \tag{1}$$

$$\mu = \beta_{0\mu} \begin{pmatrix} CRU \\ NASPA \\ Gridmet \\ MRI \\ MIROC \end{pmatrix} + \beta_{1\mu} f_{s\_\mu} \begin{pmatrix} CRU \\ NASPA \\ X_{month}, Gridmet \\ MRI \\ MIROC \end{pmatrix} + \beta_{2\mu} f_{te\_\mu}(X_{year}, X_{month}) \tag{2}$$

$$\frac{1}{\log(\alpha)} = \beta_{0\alpha} + \beta_{0\alpha} f_{s\_\alpha} \begin{pmatrix} CRU \\ NASPA \\ Gridmet \\ MRI \\ MIROC \end{pmatrix} + \beta_{1\alpha} f_{s\_\alpha} \begin{pmatrix} CRU \\ NASPA \\ X_{month}, Gridmet \\ MRI \\ MIROC \end{pmatrix} + \beta_{2\alpha} f_{te\_\alpha}(X_{year}, X_{month}) \tag{3}$$

CRU precipitation was considered 'ground truth' for bias correction because it is a land-based observation dataset that has undergone validation. Biases are assumed stationary through time; thereby bias estimated during the overlapping period with CRU will remain constant over the entire record length. This bias correction approach is similar to quantile mapping (Lanzante et al., 2018), as the *f(X_{month}, by = model)* terms adjust the distribution mean and shape parameters, with the added spline constraint that limits bias correction from changing dramatically month to month.

2.4. Significance tests

Significance testing was based on gamma distribution comparisons, always using 1840-1860 as the pre-Industrial climatology (IPCC, 2014). The null hypothesis assumed that current (2000-

2020) or future (2080-2100) precipitation values for SPI = ±1.5 were equivalent to pre-Industrial values. 10,000 random samples of the mean and shape parameter were taken from the modeled distributions of the pre-Industrial and comparison time period to capture parameter uncertainty while accounting for covariance. The significance of shifts in the precipitation extremes was determined by a two-tailed test in which the null hypothesis was rejected when more than 97.5% of random samples agreed with the sign of precipitation difference. This method is conceptually similar to a two-tailed paired t-test with α=0.05 but uses random samples from modeled distributions (Chow, 1960).

3. Results

3.1. Anthropogenic Period (1850-2100 CE) Trends

First, we examined modern changes in the 3-month drought and pluvial precipitation (SPI = ±1.5), by comparing current (2000-2020) and future (2080-2100) time slices from the NSPI model to the recent pre-Industrial baseline (1840-1860) (Figs. 1 and 2). For most regions and seasons, pluvial precipitation has increased (Fig. 2), while droughts have become drier (Fig. 1), with these trends projected to worsen throughout the next century regardless of emissions scenario. This pattern of intensifying both extremes, less precipitation during drought years and more precipitation during pluvials, is especially apparent in the Central and Eastern US. Pluvial intensification is most common during winter (NDJ) and spring (FMA) (Fig. 2), while drought intensification is most spatially extensive during summer (MJJ) and fall (ASO) (Fig. 1).

Not all regions show intensification of both extremes, instead experiencing exclusively wetter or drier trends. Mexico and the southwestern US have become drier for both drought and pluvial extremes across most seasons, with the most consistently significant decreases during drought years . Conversely, eastern Canada has/will become wetter at both extremes, most substantially during cool seasons (NDJ and FMA), resulting in worsening pluvials, but lessening droughts.

Pluvial and drought trends form spatially consistent regions despite all grid cells being modeled independently. That is, trends do not change radically over short distances, but rather transition smoothly in space. This lends further support to the findings, showing a strong spatiotemporal signal that stands apart from random noise, despite independent calibration. The specific 3-

171 month periods displayed here were chosen to align with the NASPA seasons (MJJ, DJFMA)
172 (Stahle et al., 2020).
173
174 Cool season droughts follow a distinct latitudinal breakpoint, with lessening winter drought
175 above 40°N and worsening winter drought below 40°N (Fig. 1, top rows), reminiscent of
176 latitudinal gradients noted previously for the western US (Swain et al., 2018). Lessening winter
177 drought is most notable in Eastern Canada, where winter drought precipitation is projected to
178 increase by almost 50% for both future scenarios. Mexico and the southwestern US have already
179 experienced significant intensification of winter drought and is projected to worsen, reducing
180 precipitation amounts associated with a moderate/severe drought (SPI= -1.5) by almost 100%
181 relative to 1840-1860 climatology (Fig. 1). The trend towards lessening cool season drought
182 extremes is not statistically significant to date, but is projected to become significant by the end
183 of the century, whereas the trend towards worsening winter drought extremes across much of
184 southern North America has already shown significant changes relative to pre-Industrial
185 climatology.
186 During warm seasons (MJJ and ASO), the region of worsening drought expands to cover much
187 of North America (Fig. 1), but showing relatively smaller change. Mexico, the southwestern US,
188 and the Caribbean show especially significant warm season drought precipitation decreases. This
189 is particularly deleterious when considered alongside their significant cool season drought
190 intensification, leading to drought intensification throughout the year. Because these regions rely
191 on the warm season North American Monsoon (July -September) for a majority of their annual
192 precipitation (Grantz et al., 2007), intensified warm season drought increases risks of water
193 shortage by failing to refill reservoirs. Some exceptions to the worsening warm season drought
194 trend exist (northern intermountain western US and central Mexico plateau), which may be
195 related to the spatial complexity of mountainous precipitation (Preece et al., 2021).

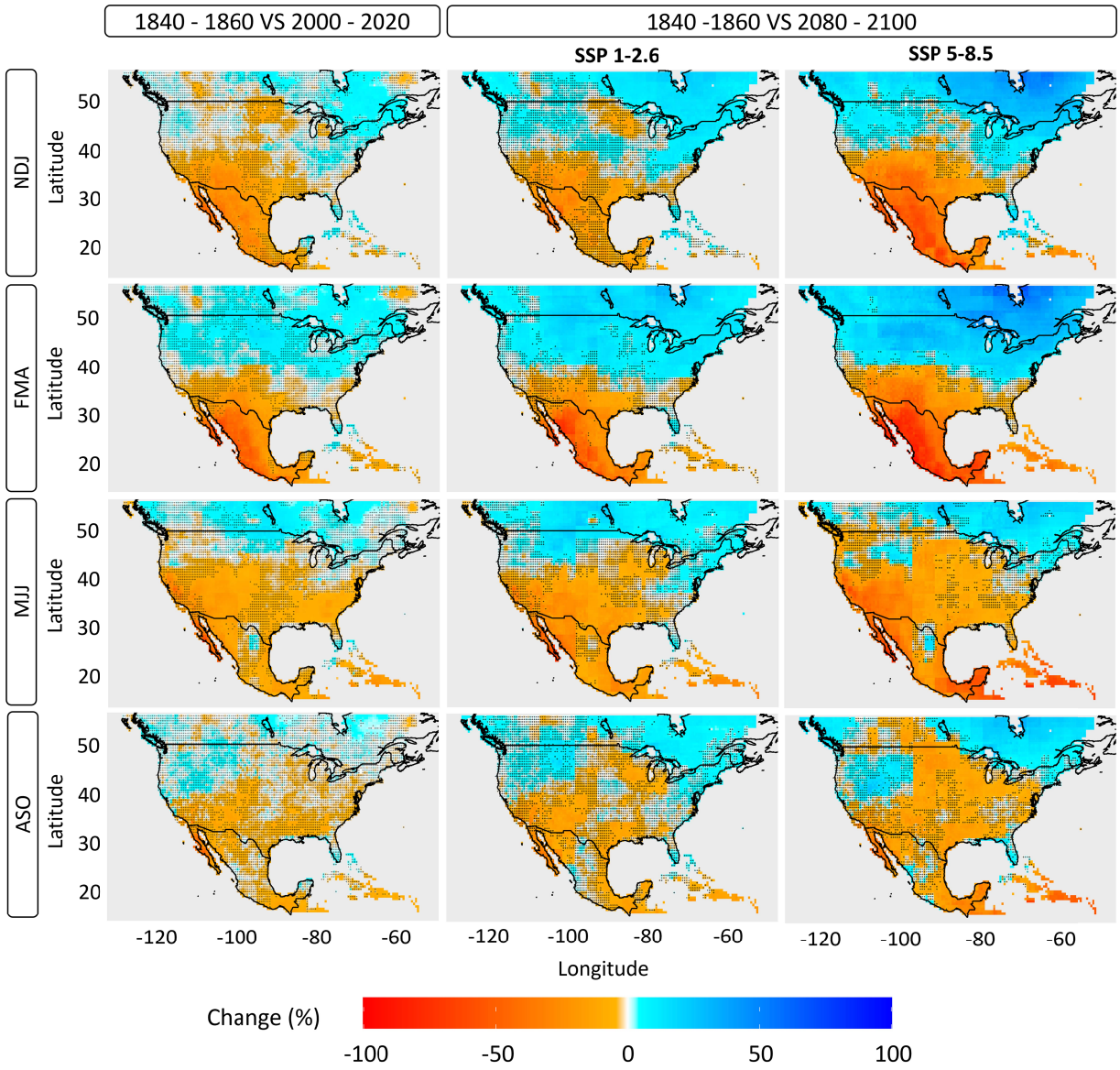

Figure 1. Percent precipitation change compared to pre-Industrials for drought years (SPI = -1.5). (left): current era (center) future under ssp1-2.6, (right) ssp5-8.5 scenarios.

Pluvials have intensified for most of North America (Fig. 2), except for Mexico and the southwestern US, particularly during cool seasons. The intensification of cool season pluvials is most significant across eastern North America, with this region expanding to cover much of the US and Canada during future scenarios (Fig. 2, top rows). While trends in the eastern US and Canada are more spatially homogenous, we note that the strongest winter pluvial intensification in the west occurs in mountainous topography during the early spring (FMA).

206 During the MJJ early summer period, the region of decreasing wet extremes expands northward
207 centered on the southwestern US. With increasing CO_2 forcing, this trend intensifies in
208 magnitude and expands spatially to include the American Plains and the Caribbean. Our finding
209 of a decrease in MJJ pluvials followed by little change during ASO mirrors previous findings of
210 a seasonal delay in the North American Monsoon under climate change (B. I. Cook & Seager,
211 2013; Pascale et al., 2017; Prein et al., 2022).
212
213 For all locations, future scenarios are extensions of the last century with no notable sign changes
214 between 2020 and 2100. Trends for many regions are already statistically significant during the
215 instrumental period (1850-2020) and where they are not, trends often become significant under
216 one or both future climate change scenarios. This implies that climate change has begun to
217 affect precipation in a manner consistent with GCM simulations under increased greenhouse gas
218 concentrations and is likely to become more intense and detectable through the 21st century.
219

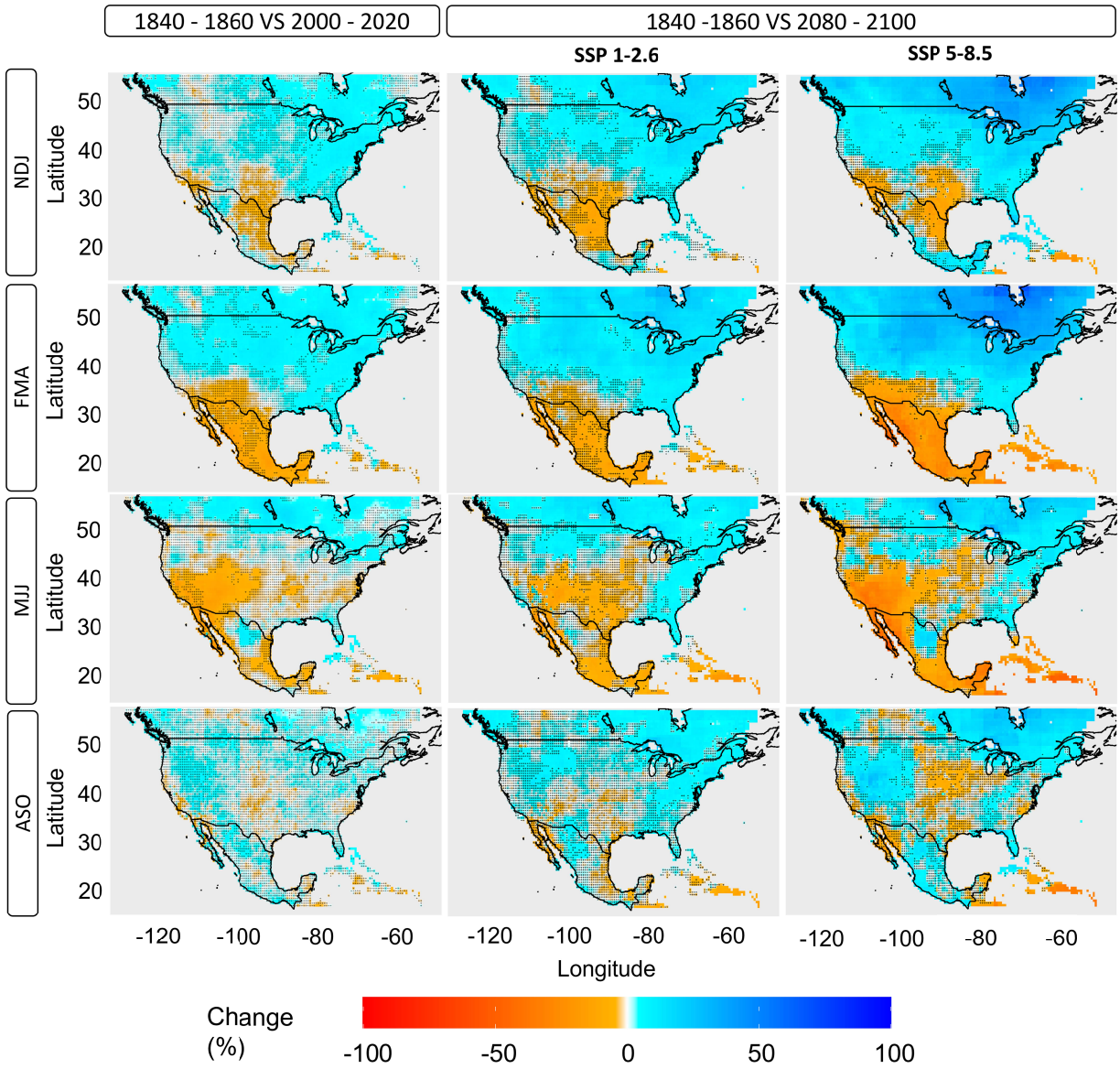

Figure 2. Percent precipitation changes compared to pre-Industrials for pluvial years (SPI = +1.5). (left) current era (center) future under ssp1-2.6, (right) ssp5-8.5 scenarios.

3.2. Millenium-Scale (850-2100 CE) Context

The ability to consider non-linear precipitation patterns in a longer context of natural climate variability using the full 1,250-year model is a major benefit of our approach. Using identical drought and pluvial definitions for several representative locations (Fig. 3, 4, S1 and S2), we find similar patterns: cool season wetting trends and warm season drying trends for northern locations

(Figs 3 and S1, top row), intensified pluvials and drought in mid-latitude region between 30º- 40º latitude (mid row), and severe drying trends in the south (bottom row).

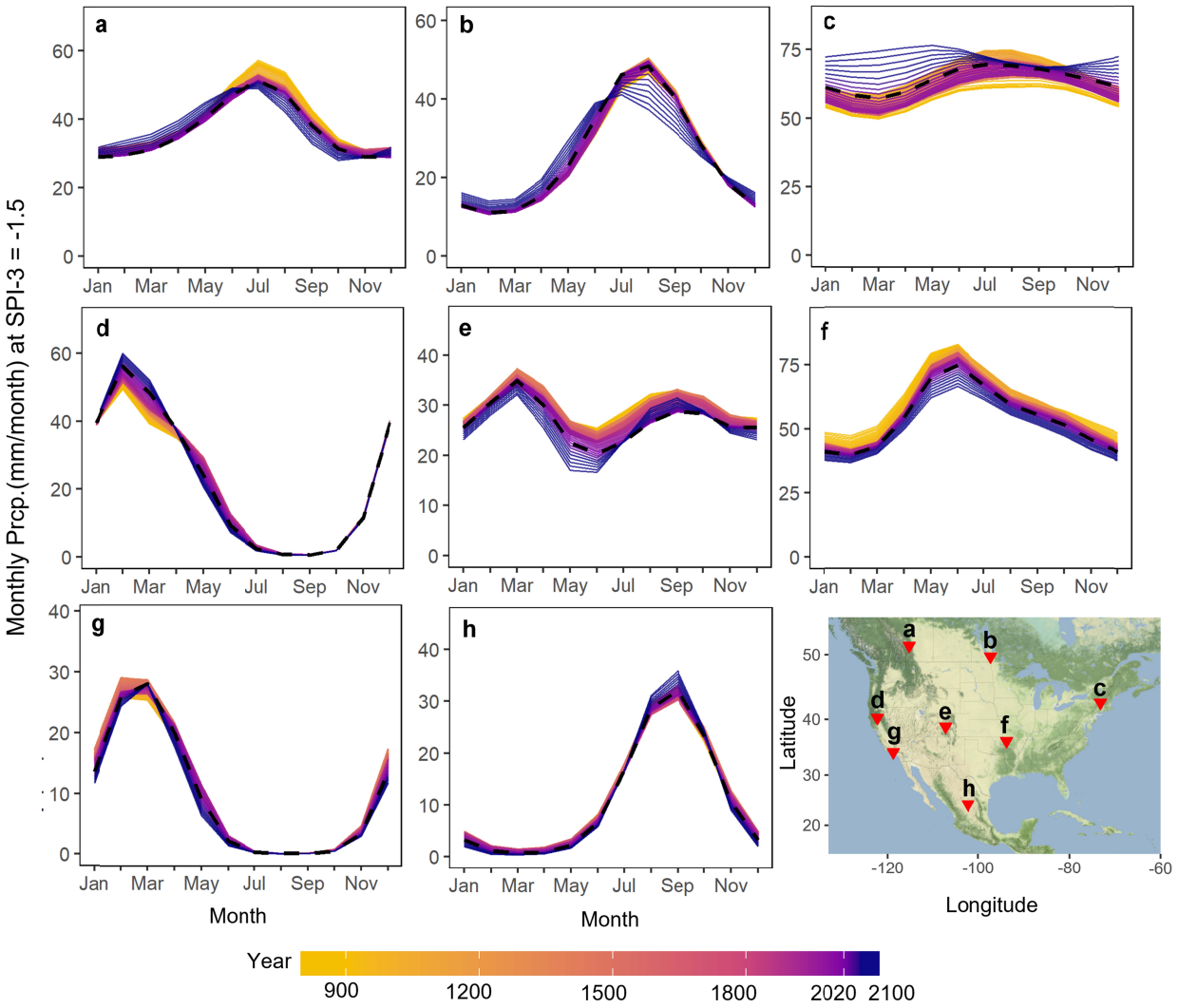

Figure 3. Seasonal precipitation in long-term trends at SPI = -1.5 for a single grid cell. Panels are organized spatially, with labels corresponding to the map in the bottom right. x-axis: the final month of the SPI-3 period (i.e., May :Mar-May precipitation rates). All future changes are modeled using the SSP 5-8.5 scenario.

For the three northern reference sites (Figs. 3 and S1, a-c) shows weaken in seasonality as overall precipitation during the winter dry season (Jan - Apr) becomes wetter, while the summer wet season (Jul - Sep) becomes drier. These phenomenon also captured in Figs S2 and S3. Unlike the northern sites, the two mid-latitude reference sites in the center of the continent (Figs. 3e and 3f) exhibit wetter pluvials and drier droughts for all seasons. This greatly increases the interannual variability for the region, fluctuating between increasingly wider extremes. Despite some natural

pre-Industrial fluctuation, the most extreme shifts for all of these sites occur after 1850, further emphasizing that modern and projected precipitation shifts are outside pre-Industrial (850-1850 CE) natural variability, as tested in Figs. 1 and 2.

The southern-most reference site, Mexico City (Fig. 3h), exhibits a shift towards drier conditions for both drought and pluvial years across most seasons, with the most dramatic changes occurring during the wet season (Jul-Sep). In future projections under high emissions scenarios, drought year precipitation is nearly 50% of the pre-Industrial, with decreases already emerging in the present (2020).

Northern and southern California, shown to the far left (Figs. 3d and g), both exhibit modern (post 1850) decrease in spring and early summer precipitation, with this trend particularly intense in Southern California. Modern drought decreases in Southern California continue throughout the summer and into the fall, whereas no equivalent trends exhist in northern California (Fig 1). Finally, both northern and southern California have experienced a long trend towards increased pluvial year precipitation during the wet winter season beginning well before the Industrial period (ca 1100 CE) (Figs 3 and 4). To better illustrate centennial-scale shifts in southern California precipitation, we examine the wet season pluvial increase (JFM), and the notable drying of the summer shoulder season (MJJ) (Fig 4).

JFM pluvial increases run counter to the overwhelming drying trend in southern California and the surrounding region, as indicated by a rightward shift in the distribution's upper tail and an increase in the upper bound through time (Fig 4a). This winter pluvial wetting trend occurred gradually over the last millennium, since 1000 CE, with no detectable acceleration during the Industrial period or into the future. The cool season in southern California is where NASPA has the best cross-validation skill (Stahle et al., 2020), lending confidence to these findings. Others have simulated relatively little change in extremely wet seasons during the 1900s and increases by 2100 (Swain et al., 2018), though our findings suggest this trend may be part of a gradual pluvial increase beginning centuries prior. It should be noted that the gradual precipitation increase for JFM pluvials is not reflected during drought years, which instead show a

precipitation decrease, widening the gap between wet and dry years during the critical winter precipitation period.

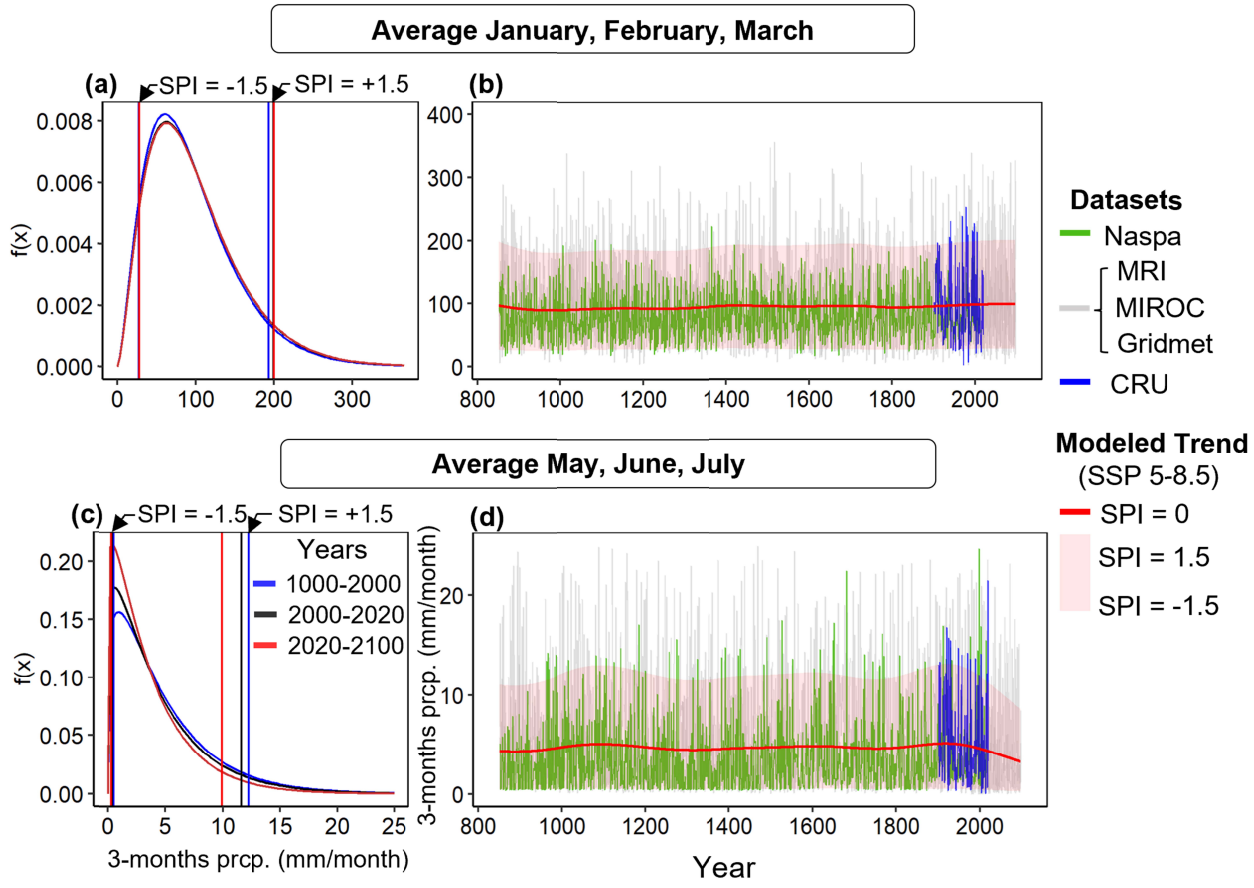

Figure 4. Modeled precipitation changes at Los Angeles, CA, USA. (Left) Fitted Gamma distributions for different periods with drought and pluvial thresholds. (Right) time series of underlying data, the bias-corrected mean, drought and pluvial thresholds.

A severe decrease in southern California precipitation occurs during the early summer MJJ season (Figs 3g and 4c), with modern climatology (black) slightly drier than pre-Industrial conditions (blue), whereas future extremes (red) indicate rapidly decreasing precipitation. While the model does not explicitly consider zero precipitation years, a detectable shift towards the zero bound suggests an increase in the frequency of years with zero precipitation during the MJJ season. Large decreases also occur in the upper tail, indicating less early summer precipitation even during particularly wet years. This decreasing trend is sudden and stands out from the prior thousand years of natural climate variability (Fig. 4d), suggesting an anthropogenic cause.

Considered together, southern California has experienced a gradual increase in wet season pluvials and a sudden 20th century decrease in spring and early summer precipitation, which generally agrees with prior studies indicating intensifying seasonality and extremes (Persad et al., 2020; Swain et al., 2018; Williams et al., 2022). This intensification complicates regional water management already experiencing a decade long drought (Diffenbaugh et al., 2015; Williams et al., 2020). Precipitation decreases during the spring and early summer lengthens the duration of the summer dry season, increasing reliance on reservoir storage accumulated during the wet period from three distinct source areas: northern California's Sierra Nevada mountains, the Colorado River, and locally (Pagán et al., 2016; Woodhouse et al., 2020). Increasing annual variability make Sierra Nevada and local sources more uncertain (Fig. 3d and g), whereas the Colorado River Basin is projected to undergo dramatic decreases over the next century (Fig. 1 and 2), further exacerbating water management risks.

4. Discussions and Conclusions

The approach used here, integrating datasets from the past through the future, relies on a novel use of hierarchical spline models (Sung et al., 2022) to provide a comprehensive view of modern and projected drought and pluvial extremes in the context of centuries of pre-industrial climate. By considering overlapping data types, distribution shifts only become significant when consistent across multiple sources and decades. Thus, GCM simulations support NASPA reconstruction skill gaps, like the northeast cool season or the ASO interpolated season (Stahle et al., 2020), while integrative splines improved parameter stability. Spatial agreement across thousands of independently modeled cells provides further confidence in these findings.

Our results highlight many regions which experienced sharp hydroclimate trends during the 20th and 21st centuries relative to a largely stable precipitation climatology during the prior 1,000 years. Drier summer droughts and wetter winter pluvials are typical across much of North America, particularly in the east and north. Unlike these regions with wider interannual variability, the south and southwest show consistent drying trends, while the far northeast and eastern Canada exhibit consistent wetting trends. Our findings agree with prior studies suggesting that climate change has intensified the hydrologic cycle, worsening drought risks

during historical dry seasons (Chou et al., 2013; Dai, 2013; Diffenbaugh et al., 2015; Lehner et al., 2018) and increasing pluvial magnitudes during wet seasons for many regions (Diffenbaugh & Davenport, 2021; Swain et al., 2018) with projected future intensification. Increases in interannual variability for mid-latitude regions and rapid trends toward dryer[wetter] conditions in the south[north] with more intense extremes makes water management more challenging as infrastructure and strategies developed in the early or mid-1900s using that time's climatology is often no longer representative of current or future climate extremes (Gangopadhyay et al., 2022; Mallakpour et al., 2019). We expect our study contributes to water infrastructure adaptation to a "new climate normal" (Hoylman et al., 2022) through improved quantification of hydroclimatic trends placed into a millenial-scale context.

Acknowledgments

This work was supported by the National Science Foundation Project No. 2002539, Byrd Polar and Climate Research Center, and the Ohio Supercomputer Center.

Open Research

NASPA data is available at https://www.ncei.noaa.gov/pub/data/paleo/treering/reconstructions/northamerica/NASPA/. CRU and GridMET datasets are available at https://crudata.uea.ac.uk/cru/data/hrg/index.htm#current and https://www.climatologylab.org/gridmet.html, respectively. GCM datsets (MIROC-ES2L and MRI-ESM2) can be downloaded from https://esgf-node.llnl.gov/search/cmip6/. The Non-stationary SPI modeling used 'mgcv' packages(Wood, 2008) in R. All code is preserved at https://doi.org/10.5281/zenodo.7789830.

345

346

347 ## References

348 Abatzoglou, J. T. (2013). Development of gridded surface meteorological data for ecological applications and
349 modelling. *International Journal of Climatology*, *33*(1), 121–131. https://doi.org/10.1002/joc.3413
350 Ault, T. R. (2020). On the essentials of drought in a changing climate. *Science*, *368*(6488), 256–260.
351 https://doi.org/10.1126/science.aaz5492
352 Bishop, D. A., Williams, A. P., Seager, R., Cook, E. R., Peteet, D. M., Cook, B. I., et al. (2021). Placing the east-
353 west North American aridity gradient in a multi-century context. *Environmental Research Letters*, *16*(11),
354 114043. https://doi.org/10.1088/1748-9326/ac2f63
355 Chou, C., Chiang, J. C. H., Lan, C.-W., Chung, C.-H., Liao, Y.-C., & Lee, C.-J. (2013). Increase in the range
356 between wet and dry season precipitation. *Nature Geoscience*, *6*(4), 263–267.
357 https://doi.org/10.1038/ngeo1744
358 Chow, G. C. (1960). Tests of Equality Between Sets of Coefficients in Two Linear Regressions. *Econometrica*,
359 *28*(3), 591–605. https://doi.org/10.2307/1910133
360 Cook, B., Seager, R., Williams, A. P., Puma, M. J., McDermid, S., Kelley, M., & Nazarenko, L. (2019). Climate
361 Change Amplification of Natural Drought Variability: The Historic Mid-Twentieth-Century North
362 American Drought in a Warmer World. *Journal of Climate*, *32*(17), 5417–5436.
363 https://doi.org/10.1175/JCLI-D-18-0832.1
364 Cook, B. I., & Seager, R. (2013). The response of the North American Monsoon to increased greenhouse gas
365 forcing. *Journal of Geophysical Research: Atmospheres*, *118*(4), 1690–1699.
366 https://doi.org/10.1002/jgrd.50111
367 Cui, T., Li, C., & Tian, F. (2021). Evaluation of Temperature and Precipitation Simulations in CMIP6 Models Over
368 the Tibetan Plateau. *Earth and Space Science*, *8*(7), e2020EA001620.
369 https://doi.org/10.1029/2020EA001620
370 Dai, A. (2013). Increasing drought under global warming in observations and models. *Nature Climate Change*, *3*(1),
371 52–58. https://doi.org/10.1038/nclimate1633

372 Diffenbaugh, N. S., & Davenport, F. V. (2021). On the impossibility of extreme event thresholds in the absence of
373 global warming. *Environmental Research Letters*, *16*(11), 115014. https://doi.org/10.1088/1748-
374 9326/ac2f1a
375 Diffenbaugh, N. S., Swain, D. L., & Touma, D. (2015). Anthropogenic warming has increased drought risk in
376 California. *Proceedings of the National Academy of Sciences*, *112*(13), 3931–3936.
377 https://doi.org/10.1073/pnas.1422385112
378 Diffenbaugh, N. S., Singh, D., Mankin, J. S., Horton, D. E., Swain, D. L., Touma, D., et al. (2017). Quantifying the
379 influence of global warming on unprecedented extreme climate events. *Proceedings of the National*
380 *Academy of Sciences*, *114*(19), 4881–4886. https://doi.org/10.1073/pnas.1618082114
381 Eyring, V., Bony, S., Meehl, G. A., Senior, C. A., Stevens, B., Stouffer, R. J., & Taylor, K. E. (2016). Overview of
382 the Coupled Model Intercomparison Project Phase 6 (CMIP6) experimental design and organization.
383 *Geoscientific Model Development*, *9*(5), 1937–1958. https://doi.org/10.5194/gmd-9-1937-2016
384 Gangopadhyay, S., Clark, M., & Rajagopalan, B. (2005). Statistical downscaling using K-nearest neighbors. *Water*
385 *Resources Research*, *41*(2). https://doi.org/10.1029/2004WR003444
386 Gangopadhyay, S., Woodhouse, C. A., McCabe, G. J., Routson, C. C., & Meko, D. M. (2022). Tree Rings Reveal
387 Unmatched 2nd Century Drought in the Colorado River Basin. *Geophysical Research Letters*, *49*(11),
388 e2022GL098781. https://doi.org/10.1029/2022GL098781
389 Grantz, K., Rajagopalan, B., Clark, M., & Zagona, E. (2007). Seasonal Shifts in the North American Monsoon.
390 *Journal of Climate*, *20*(9), 1923–1935. https://doi.org/10.1175/JCLI4091.1
391 Hajima, T., Watanabe, M., Yamamoto, A., Tatebe, H., Noguchi, M. A., Abe, M., et al. (2020). Development of the
392 MIROC-ES2L Earth system model and the evaluation of biogeochemical processes and feedbacks.
393 *Geoscientific Model Development*, *13*(5), 2197–2244. https://doi.org/10.5194/gmd-13-2197-2020
394 Harris, I., Osborn, T. J., Jones, P., & Lister, D. (2020). Version 4 of the CRU TS monthly high-resolution gridded
395 multivariate climate dataset. *Scientific Data*, *7*(1), 109. https://doi.org/10.1038/s41597-020-0453-3
396 Heim, R. R. (2002). A Review of Twentieth-Century Drought Indices Used in the United States. *Bulletin of the*
397 *American Meteorological Society*, *83*(8), 1149–1166. https://doi.org/10.1175/1520-0477-83.8.1149
398 Ho, M., Lall, U., Allaire, M., Devineni, N., Kwon, H. H., Pal, I., et al. (2017). The future role of dams in the United
399 States of America. *Water Resources Research*, *53*(2), 982–998. https://doi.org/10.1002/2016WR019905

Hoylman, Z. H., Bocinsky, R. K., & Jencso, K. G. (2022). Drought assessment has been outpaced by climate change: empirical arguments for a paradigm shift. *Nature Communications*, *13*(1), 2715. https://doi.org/10.1038/s41467-022-30316-5

IPCC. (2014). *Climate Change 2013: The Physical Science Basis: Working Group I Contribution to the Fifth Assessment Report of the Intergovernmental Panel on Climate Change*. Cambridge University Press.

Lanzante, J. R., Dixon, K. W., Nath, M. J., Whitlock, C. E., & Adams-Smith, D. (2018). Some Pitfalls in Statistical Downscaling of Future Climate. *Bulletin of the American Meteorological Society*, *99*(4), 791–803. https://doi.org/10.1175/BAMS-D-17-0046.1

Lehner, F., Coats, S., Stocker, T. F., Pendergrass, A. G., Sanderson, B. M., Raible, C. C., & Smerdon, J. E. (2017). Projected drought risk in 1.5°C and 2°C warmer climates. *Geophysical Research Letters*, *44*(14), 7419–7428. https://doi.org/10.1002/2017GL074117

Lehner, F., Deser, C., Simpson, I. R., & Terray, L. (2018). Attributing the U.S. Southwest's Recent Shift Into Drier Conditions. *Geophysical Research Letters*, *45*(12), 6251–6261. https://doi.org/10.1029/2018GL078312

Mallakpour, I., AghaKouchak, A., & Sadegh, M. (2019). Climate-Induced Changes in the Risk of Hydrological Failure of Major Dams in California. *Geophysical Research Letters*, *46*(4), 2130–2139. https://doi.org/10.1029/2018GL081888

Marvel, K., Cook, B. I., Bonfils, C., Smerdon, J. E., Williams, A. P., & Liu, H. (2021). Projected Changes to Hydroclimate Seasonality in the Continental United States. *Earth's Future*, *9*(9), e2021EF002019. https://doi.org/10.1029/2021EF002019

Pagán, B. R., Ashfaq, M., Rastogi, D., Kendall, D. R., Kao, S.-C., Naz, B. S., et al. (2016). Extreme hydrological changes in the southwestern US drive reductions in water supply to Southern California by mid century. *Environmental Research Letters*, *11*(9), 094026. https://doi.org/10.1088/1748-9326/11/9/094026

Pascale, S., Boos, W. R., Bordoni, S., Delworth, T. L., Kapnick, S. B., Murakami, H., et al. (2017). Weakening of the North American monsoon with global warming. *Nature Climate Change*, *7*(11), 806–812. https://doi.org/10.1038/nclimate3412

Pedersen, E. J., Miller, D. L., Simpson, G. L., & Ross, N. (2019). Hierarchical generalized additive models in ecology: an introduction with mgcv. *PeerJ*, *7*, e6876. https://doi.org/10.7717/peerj.6876

427 Persad, G. G., Swain, D. L., Kouba, C., & Ortiz-Partida, J. P. (2020). Inter-model agreement on projected shifts in
428 California hydroclimate characteristics critical to water management. *Climatic Change*, *162*(3), 1493–1513.
429 https://doi.org/10.1007/s10584-020-02882-4
430 Preece, J. R., Shinker, J. J., Riebe, C. S., & Minckley, T. A. (2021). Elevation-dependent precipitation response to El
431 Niño-Southern oscillation revealed in headwater basins of the US central Rocky Mountains. *International*
432 *Journal of Climatology*, *41*(2), 1199–1210. https://doi.org/10.1002/joc.6790
433 Prein, A. F., Towler, E., Ge, M., Llewellyn, D., Baker, S., Tighi, S., & Barrett, L. (2022). Sub-Seasonal
434 Predictability of North American Monsoon Precipitation. *Geophysical Research Letters*, *49*(9),
435 e2021GL095602. https://doi.org/10.1029/2021GL095602
436 Stagge, J. H., & Sung, K. (2022). A Non-stationary Standardized Precipitation Index (NSPI) using Bayesian Splines.
437 *Journal of Applied Meteorology and Climatology*, *1*(aop). https://doi.org/10.1175/JAMC-D-21-0244.1
438 Stahle, D. W., Cook, E. R., Burnette, D. J., Torbenson, M. C. A., Howard, I. M., Griffin, D., et al. (2020).
439 Dynamics, Variability, and Change in Seasonal Precipitation Reconstructions for North America. *Journal*
440 *of Climate*, *33*(8), 3173–3195. https://doi.org/10.1175/JCLI-D-19-0270.1
441 Stevenson, S., Coats, S., Touma, D., Cole, J., Lehner, F., Fasullo, J., & Otto-Bliesner, B. (2022). Twenty-first
442 century hydroclimate: A continually changing baseline, with more frequent extremes. *Proceedings of the*
443 *National Academy of Sciences*, *119*(12), e2108124119. https://doi.org/10.1073/pnas.2108124119
444 Sung, K., Torbenson, M. C. A., & Stagge, J. H. (2022). Assessing decadal to centennial scale nonstationary
445 variability in meteorological drought trends. *Hydrology and Earth System Sciences*, *EGUsphere*.
446 https://doi.org/10.5194/egusphere-2022-476
447 Swain, D. L., Langenbrunner, B., Neelin, J. D., & Hall, A. (2018). Increasing precipitation volatility in twenty-first-
448 century California. *Nature Climate Change*, *8*(5), 427–433. https://doi.org/10.1038/s41558-018-0140-y
449 Williams, A. P., Cook, E. R., Smerdon, J. E., Cook, B. I., Abatzoglou, J. T., Bolles, K., et al. (2020). Large
450 contribution from anthropogenic warming to an emerging North American megadrought. *Science*,
451 *368*(6488), 314–318. https://doi.org/10.1126/science.aaz9600
452 Williams, A. P., Cook, B. I., & Smerdon, J. E. (2022). Rapid intensification of the emerging southwestern North
453 American megadrought in 2020–2021. *Nature Climate Change*, *12*(3), 232–234.
454 https://doi.org/10.1038/s41558-022-01290-z

455 Wood, S. N. (2008). Fast stable direct fitting and smoothness selection for generalized additive models. *Journal of*
456 *the Royal Statistical Society: Series B (Statistical Methodology)*, *70*(3), 495–518.
457 https://doi.org/10.1111/j.1467-9868.2007.00646.x
458 Woodhouse, C. a., Meko, D. m., & Bigio, E. r. (2020). A Long View of Southern California Water Supply: Perfect
459 Droughts Revisited. *JAWRA Journal of the American Water Resources Association*, *56*(2), 212–229.
460 https://doi.org/10.1111/1752-1688.12822
461 Yukimoto, S., Kawai, H., Koshiro, T., Oshima, N., Yoshida, K., Urakawa, S., et al. (2019). The Meteorological
462 Research Institute Earth System Model Version 2.0, MRI-ESM2.0: Description and Basic Evaluation of the
463 Physical Component. *Journal of the Meteorological Society of Japan. Ser. II*, *advpub*, 2019–051.
464 https://doi.org/10.2151/jmsj.2019-051
465